

Correlation between local vibrations and metal mass in AlB_2 -type transition-metal diborides

W. S. Chu,^a S. Zhang,^{a,b} M. J. Yu,^a L. R. Zheng,^a T. D. Hu,^a H. F. Zhao,^a A. Marcelli,^c A. Bianconi,^d N. L. Saini,^d W. H. Liu^b and Z. Y. Wu^{a,b,e*}

^aBeijing Synchrotron Radiation Facility, Institute of High Energy Physics, Chinese Academy of Sciences, Beijing 100049, People's Republic of China, ^bNational Synchrotron Radiation Laboratory, University of Science and Technology of China, Hefei 230026, People's Republic of China, ^cUniversità di Roma 'La Sapienza', and Unità INFN, 00185 Roma, Italy, ^dINFN – Laboratori Nazionali di Frascati, PO Box 13, 00044 Frascati, Italy, and ^eTheoretical Physics Center for Science Facilities, Chinese Academy of Sciences, Beijing 100049, People's Republic of China. E-mail: wuzy@ihep.ac.cn

Lattice vibrations have been investigated in TiB_2 , ZrB_2 and HfB_2 by temperature-dependent extended X-ray absorption fine structure (EXAFS) experiments. Data clearly show that the EXAFS oscillations are characterized by an anomalous behavior of the Debye–Waller factor of the transition-metal–boron pair, which is suggested to be associated with a superposition of an optical mode corresponding to phonon vibrations induced by the B sublattice and an acoustic mode corresponding to the transition-metal (TM) sublattice. Data can be interpreted as a decoupling of the metal and boron vibrations observed in these transition-metal diborides (TMB_2), a mechanism that may be responsible for the significant reduction of the superconducting transition temperature observed in these systems with respect to the parent MgB_2 compound. The vibrational behavior of TM–TM bonds has also been investigated to study the occurrence of anisotropy and anomalies in the lattice vibrational behavior of TM–TM bonds.

Keywords: EXAFS; diboride; superconductor.

1. Introduction

The unexpected discovery of superconductivity in MgB_2 with $T_c = 39$ K (Nagamatsu *et al.*, 2001) stimulated research in diboride compounds, a large set of materials that crystallize in the well known AlB_2 structure ($P6/mmm$) which include a large number of transition-metal (TM) compounds (Buzea & Yamashita, 2001; Ivanovskii, 2003). However, if we exclude ZrB_2 in which $T_c = 5.5$ K (Gasparov *et al.*, 2001), most of the transition-metal diborides do not exhibit superconductivity above 4 K (Buzea & Yamashita, 2001).

The superconductive mechanism is particularly interesting in MgB_2 (Hinks *et al.*, 2001; Kortus *et al.*, 2001; Yildirim *et al.*, 2001) because of the simple MgB_2 structure. Similarly, the AlB_2 -type diborides represent ideal systems to investigate superconductivity and its dependence on temperature; the TMB_2 compounds contain different metals and are characterized by a different d -state occupancy with a large mass of the TM atoms. Energy band structure calculations suggest that MgB_2 superconductivity is mainly driven by σ band holes (An & Pickett, 2001). However, among transition-metal diborides, calculations indicate that only ScB_2 and YB_2 have p_{xy} bands at the A point (Ivanovskii, 2003), *i.e.* the (0, 0, 0.5) point in the

primitive Brillouin zone, that lies above the Fermi level as in MgB_2 . Nevertheless, the hole carrier concentration for these two compounds is very small and may be the main reason for the lack of superconductivity behavior (Vajeeston *et al.*, 2001). On the other hand, the metal mass in AlB_2 -type diborides strongly affects the lattice vibration properties and contributes to the superconductive mechanism of the BCS-like superconductor MgB_2 . Osborn *et al.* (2001) and Heid *et al.* (2003) measured the phonon density of states of MgB_2 and several TMB_2 samples with inelastic neutron scattering experiments. Data show that the light mass of Mg in MgB_2 enhances the phonon frequency with respect to TMB_2 and a strong electron–phonon interaction occurs in MgB_2 . However, it is still unclear how the type and the mass of metals in the diborides modulate the lattice vibration affecting the superconductive properties of the different TMB_2 .

Temperature-dependent extended X-ray absorption fine structure (EXAFS) spectroscopy is one of the few techniques capable of providing dynamic information that can be correlated with data available by other techniques such as infrared and Raman spectroscopies or neutron scattering. Moreover, XAS spectroscopy is an element-selective probe and EXAFS experiments *versus T* may probe the vibrational properties of

the individual atomic pairs in TM diborides (Gregor & Lytle, 1979; Sevillano *et al.*, 1979; Dalba & Fornasini, 1997).

The main goal of this paper is the study of the local dynamic structure of both TM–B and TM–TM pairs for the group IV transition-metal diborides, *i.e.* TiB₂, ZrB₂ and HfB₂, by temperature-dependent EXAFS measurements. With this method both the static disorder and the phonon frequencies of TM–B and TM–TM pairs can be obtained by a quantitative analysis of the behavior of the Debye–Waller factor.

2. Experimental details

High-purity samples were prepared from stoichiometric mixtures of transition-metal and boron elements obtained from Alfa-Aesar and Sigma Aldrich. Details of the synthesis of these samples are available elsewhere (Nagamatsu *et al.*, 2001). Polycrystalline samples were found to be single phase by X-ray diffraction and none show superconductivity above 4 K.

EXAFS spectra at the transition-metal *K*-edge in TiB₂ and ZrB₂ and at the *L*₃-edge in HfB₂ were measured in transmission mode with a temperature uncertainty of ± 1 K using a Si (111) double-crystal monochromator on beamline 1W1B of the Beijing Synchrotron Radiation Facility (BSRF). The storage ring was working at 2.2 GeV with an electron current decreasing from 120 to 80 mA in the span time of 12 h. Samples were ground into fine powders and brushed onto tapes that were stacked together to give approximately one X-ray-absorption length (*i.e.* $\mu x \simeq 1$) at their corresponding metal edges. Fig. 1 shows room-temperature raw EXAFS data of TiB₂, ZrB₂ and HfB₂.

3. Results and discussion

3.1. EXAFS data analysis

Data were processed and analyzed using the *UWXAFS* package (Stern *et al.*, 1995) and with the code *WinXAS3.1* (Ressler, 1998). Both results are within the estimated uncertainties. The energy of the absorption edges was determined by the first and second derivative of the spectra and the data were normalized using the *AUTOBAK* method (Newville *et al.*, 1993). An *r* range of $r < 1.2$ Å was used to minimize the contribution below the first shell, while oscillations were weighted by k^3 to highlight the high photoelectron wavevector region for TiB₂ and by k^2 for ZrB₂ and HfB₂.

In Fig. 2 we show representative experimental k^3 - (or k^2) weighted EXAFS oscillations of the TiB₂, ZrB₂ and HfB₂ samples *versus* temperature. For all measured EXAFS of these compounds an overall damping of the oscillations occurs with increasing temperature. A clear temperature-dependent behavior is evident in Fourier transforms of the EXAFS oscillations as shown in Fig. 3. Here the Fourier transforms are compared, without phase-shift correction, at the transition-metal edges of TiB₂, ZrB₂ and HfB₂.

The crystal structure of the samples is *C*₃₂ with space-group symmetry *P6/mmm* (Nagamatsu *et al.*, 2001): a hexagonal

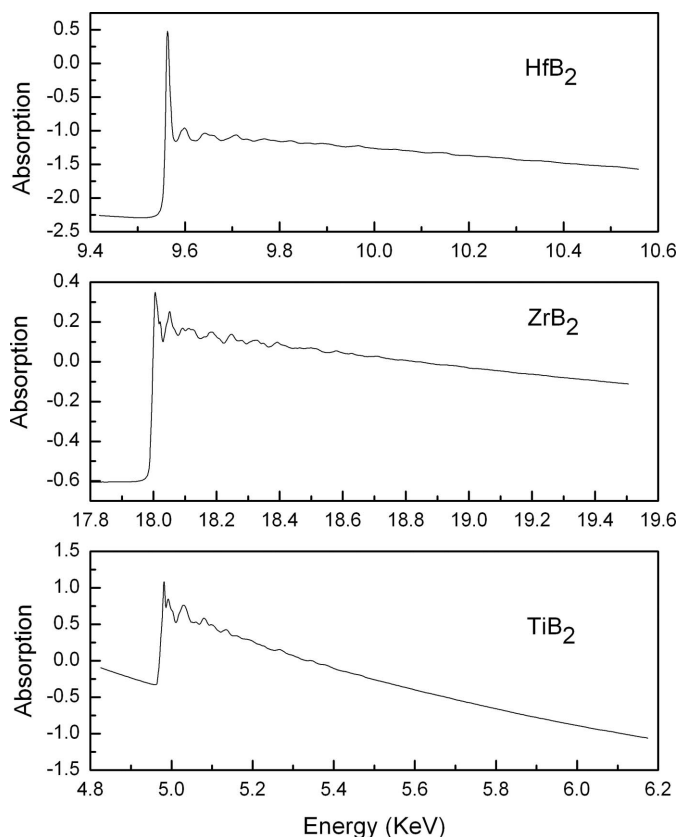


Figure 1
Room-temperature raw EXAFS data of TiB₂, ZrB₂ and HfB₂.

lattice in which close-packed transition-metal layers alternate with graphite-like B layers. Each TM atom has 12 nearest-neighbor B atoms, six nearest-neighbor TM atoms in the plane and two out of the plane. Based on the local geometry of the TM photoabsorbers, the first main peak in the Fourier transforms corresponds to the TM–B distance, *e.g.* the single-scattering contribution of the ejected photoelectron at the TM site with the nearest 12 B atoms. The second peak around 3 Å corresponds to the TM–TM single-scattering contribution, including the two subshells of the six nearest-neighbor TM atoms within the layer and denoted by TM–TM1 and the two out-of-the-plane TM atoms identified as TM–TM2. With decreasing temperature all features of the Fourier transforms, both in terms of positions and shapes, are almost unchanged implying that no phase transitions occur during cooling. The only observed effects are changes in the amplitude that decreases slightly from 28 K to 78 K and more significantly above 78 K for all single-scattering contributions.

To better reconstruct the local structure of these transition-metal diborides as a function of temperature, we carefully analyzed the EXAFS signal of the three pairs: the TM–B and the two TM–TM contributions with *FEFF8.0* (Rehr *et al.*, 1991; Zabinsky *et al.*, 1995) generating both the scattering amplitudes and the phase shifts starting from available X-ray diffraction data.

In Fig. 4 we show a representative EXAFS fit performed using the first three shells in TMB₂. Table 1 shows some non-structure parameters of the EXAFS fits for TiB₂, ZrB₂ and

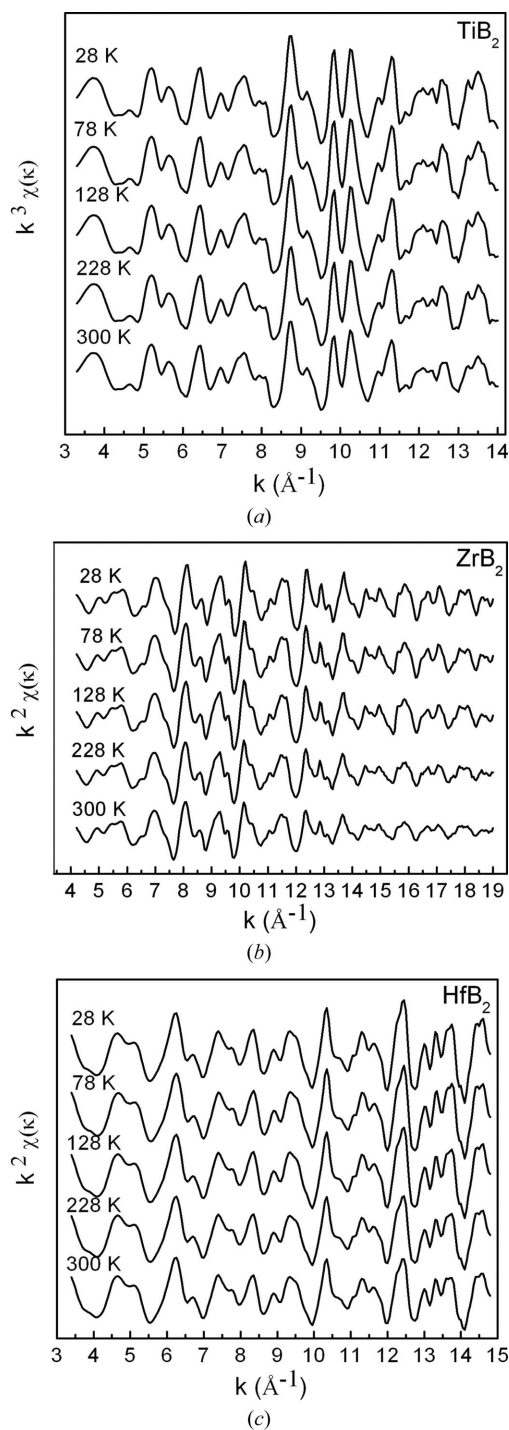


Figure 2
Weighted EXAFS oscillations as extracted from the representative transition-metal absorption spectra of (a) TiB_2 , (b) ZrB_2 and (c) HfB_2 versus temperature.

HfB_2 . The results find that all distances are independent of temperature within the experimental uncertainty. As shown in Table 2, these distances are in good agreement with X-ray diffraction data. The same analysis, as discussed below, will allow the temperature dependence of the Debye–Waller factors to be investigated as shown in Fig. 6 for the TM–B bonds (symbols) and in Fig. 7 for the two TM–TM pairs (symbols).

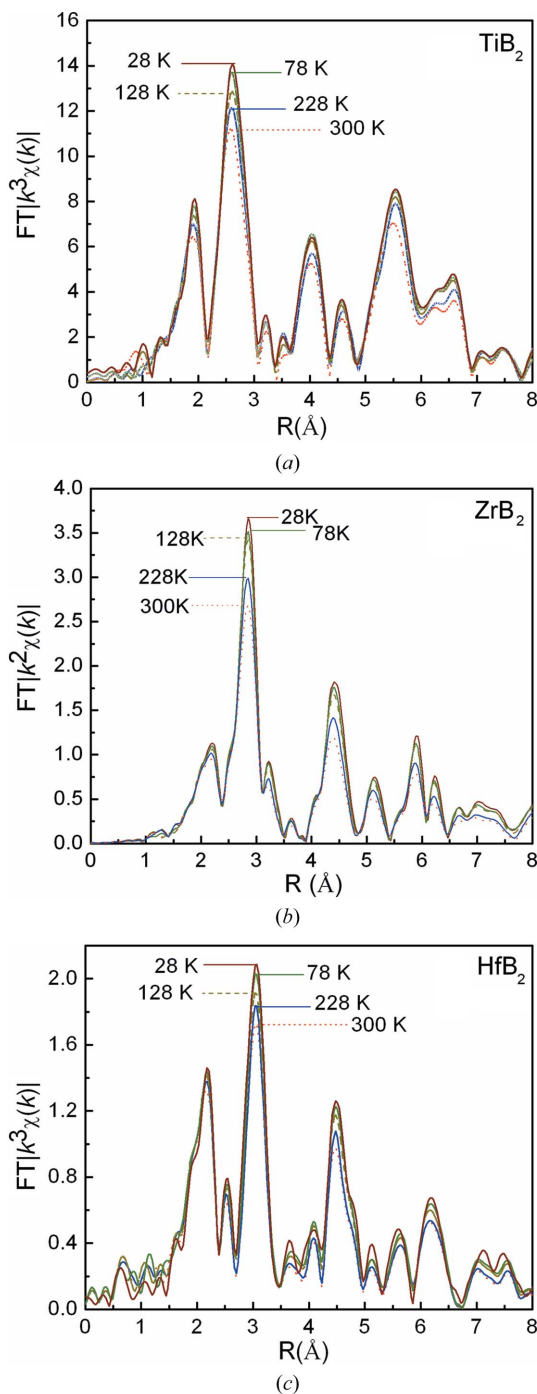


Figure 3
Comparison of the Fourier transforms, not corrected for the phase shifts, of the EXAFS spectra of TM diborides versus temperature. For all EXAFS analysis the Hanning window was used.

3.2. Localized vibration of the TM–B bonds

The Debye–Waller factor (DWF) of each shell is the sum of two contributions, *i.e.*

$$\sigma^2 = \sigma_{\text{stat}}^2 + \sigma_{\text{vib}}^2. \quad (1)$$

The first contribution is temperature independent and arises from static disorder, for example to the dispersion of bond

Table 1

Non-structure parameters of the EXAFS fits for TiB₂, ZrB₂ and HfB₂.

	<i>k</i> range	<i>R</i> range	<i>N</i> _{ind} [†]	<i>S</i> ₀ [‡]	Δ <i>E</i> ₀ [‡]	<i>R</i> factor [§]
TiB ₂	3.3–14	1.1–3.1	13	0.70	−4.0	0.0026
ZrB ₂	4–19	1.1–3.6	24	1.0	−2.0	0.0077
HfB ₂	3.6–14.8	1.4–3.4	14	0.98	8.0	0.0011

[†] $N_{\text{ind}} \simeq (2\Delta k \Delta R)/\pi$ is the number of independent data points while Δk and ΔR are the *k* and *R* intervals in which data have been analyzed, respectively. In the analysis, the total number of free parameters, *i.e.* the three radial distances and their corresponding DWFs, is smaller than N_{ind} . [‡] The effective amplitude reduction factor S_0^{\ddagger} and the photoelectron energy origin ΔE_0 are best-fit values identical for all temperatures. Both have been fixed in the final fit. [§] The *R* factor is a standard function defined by the Standards and Criteria Committee of the International XAFS Society (Lytle *et al.*, 1989). Shown here are the results of the fit of the EXAFS spectra at room temperature for each sample.

Table 2

Calculated static distortions and the two Einstein temperatures of TM–B pairs for TiB₂, ZrB₂ and HfB₂ diborides.

For comparison the corresponding vibrational frequencies are obtained by the equation $\nu' = kT_E/e$.

	Bond	<i>R</i> (Å)	σ_{stat}^2 (Å ²)	<i>T</i> _E (K)	ν' (meV)	ν (meV)
TiB ₂	Ti–B	2.37	0.0003	1376 ± 45 [†]	118.6 ± 3.9	110 [‡]
				483 ± 15	41.5 ± 1.3	40 [‡]
ZrB ₂	Zr–B	2.56	0.0012	1166 ± 40	100.3 ± 3.4	95 [§]
				279 ± 10	24.0 ± 0.9	30 [§]
HfB ₂	Hf–B	2.51	0.0013	1221 ± 45	105.0 ± 3.9	100 [‡]
				232 ± 10	20.0 ± 0.9	20 [‡]

[†] Uncertainties in the parameters were estimated by the standard EXAFS method. The quality of the fit is obtained by δ , the fractional increase of χ^2 above its minimum. [‡] Heid *et al.* (2003). [§] Naidyuk *et al.* (2002).

lengths without vibration. The second is due to thermal vibration and is correlated to the vibrational spectrum of the system. The vibrational contribution can be described by the Einstein model (Knap *et al.*, 1985) as

$$\sigma_{\text{vib}}^2 = \frac{\hbar^2}{2k\mu} \frac{1}{T_E} \coth\left[\frac{T_E}{2T}\right], \quad (2)$$

where μ is the reduced mass of the atom pair, *T* is the temperature, *k* is Boltzmann's constant and \hbar is Planck's constant. In this equation, $T_E = (\hbar/k)\omega_E$ is the Einstein temperature and ω_E is the corresponding Einstein frequency which gives a non-zero σ_{vib}^2 value at 0 K.

Lattice dynamics information is contained in the temperature dependence of the DWFs, which increase monotonically with temperature, as shown in Figs. 6 and 7. Looking at the panels of Fig. 6, the DWF of the first shell, *i.e.* the TM–B bond, is flat at low temperature and begins to increase smoothly above 50 K or at higher temperature as in TiB₂. The DWFs of these diborides cannot be described within the framework of the Einstein model whose best fits are represented by blue lines in Fig. 6. In order to illustrate the anomalous vibration behavior of these TM–B bonds, we compare in Fig. 5 the experimental DWF curve (symbols) of ZrB₂ for the Zr–B shell with simulations within the framework of the Einstein model at different Einstein temperatures. A standard DWF curve is characterized by three distinct regimes: (a) a constant region at low temperature; (b) the turning region in the intermediate range; and (c) a linear region at high temperature. Therefore,

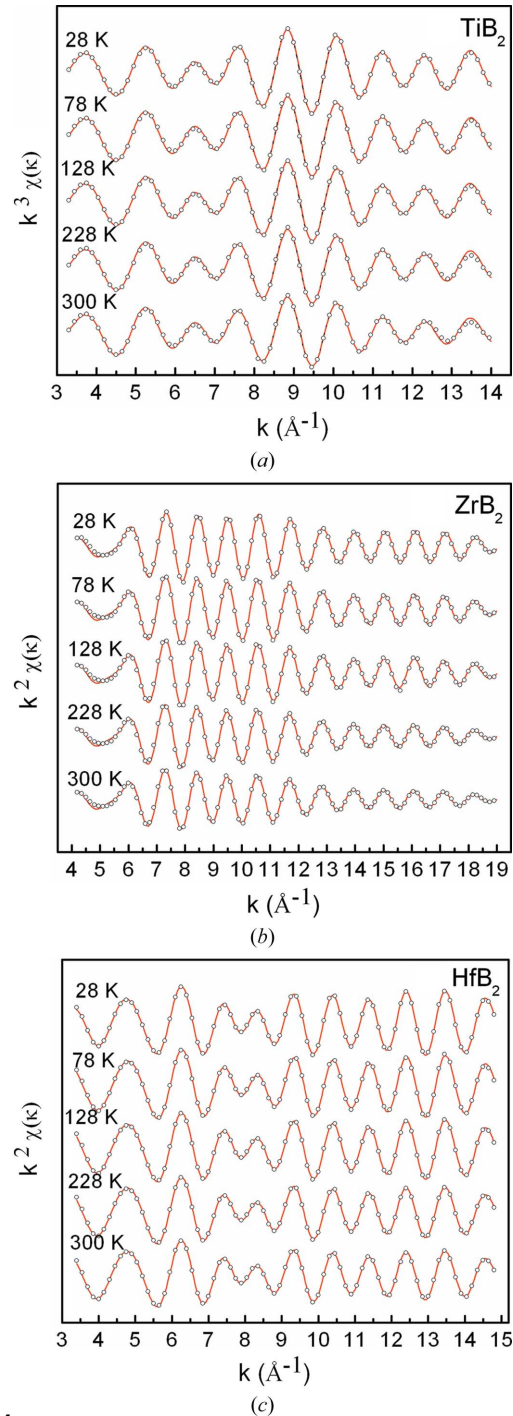


Figure 4

Comparison of experimental (circles) and fit (lines) EXAFS oscillations for the TM–B, TM–TM1 and TM–TM2 shells as extracted from the representative transition-metal absorption spectra of (a) TiB₂, (b) ZrB₂ and (c) HfB₂ versus temperature.

the DWF behavior *versus* temperature may be described using a single parameter: the turning point in the intermediate range as clearly outlined in Fig. 5. We assume that this parameter is associated only with a vibrational frequency that may be associated with the Einstein temperature of the corresponding atomic pair. If the Einstein temperature decreases, the turning point of the DWF curve shifts to lower temperature. Looking

at the simulations in Fig. 5, reasonable agreement with experimental data occurs only when the Einstein temperature is significantly lower than 200 K. This behavior suggests the possible occurrence of an additional low-frequency vibration in the Zr–B pair, associated with a higher Einstein frequency and negatively correlated to the other Zr/B atom frequency.

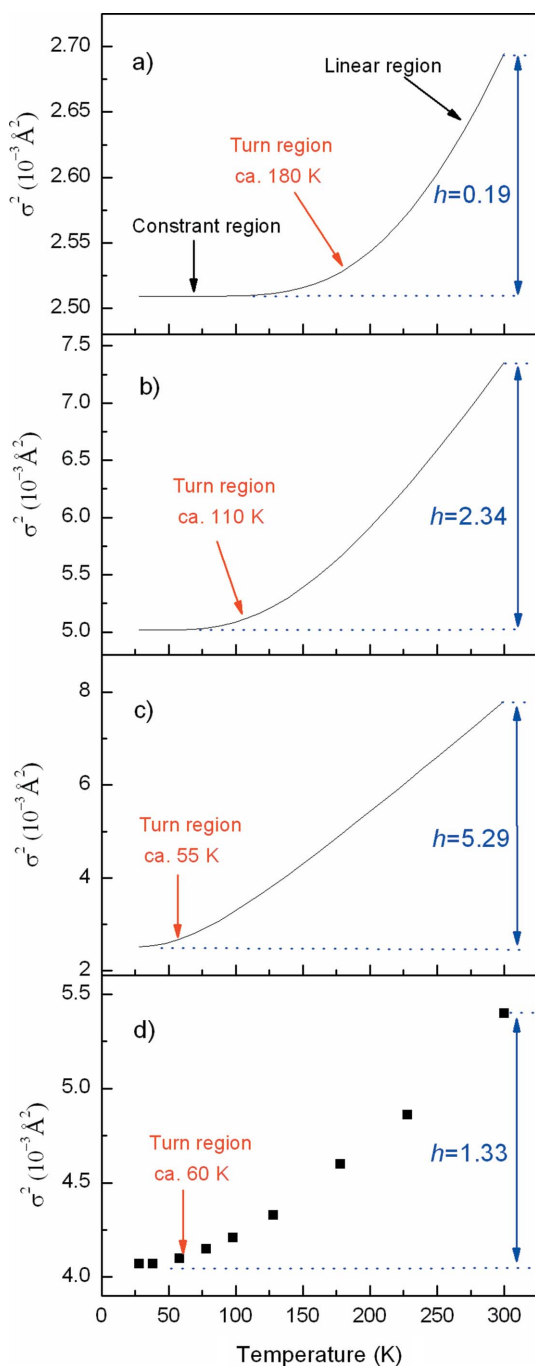


Figure 5
Comparison of DWFs calculated using the Einstein model with different Einstein temperatures: (a) $T_E = 1000$ K, (b) $T_E = 500$ K and (c) $T_E = 200$ K and experimental Debye–Waller data (d) for the Zr–B pair in the ZrB_2 system.

Table 3

Correlation between simulations and the reduced mass of the TM diborides pairs.

	a	μ	μ/a	m_B	$\mu/(1-a)$	m_{TM}
TiB_2	0.62 ± 0.05	8.820	14.23 ± 1.15	10.812	17.42 ± 1.41	47.867
ZrB_2	0.89 ± 0.08	9.666	10.86 ± 0.98	10.812	91.22 ± 8.20	87.873
HfB_2	0.92 ± 0.08	10.194	11.08 ± 0.96	10.812	178.49 ± 15.52	127.425

A similar phenomenon has been observed in Y and La (YB_6 and LaB_6) alloys by means of Raman spectroscopy (Lannin & Messier, 1980). Therefore, for diboride systems it appears impossible to fit the DWF behavior of the TM–B pair with a simple Einstein model. In order to reproduce the curve successfully, we introduce a DW description with two temperatures, T_{E1} and T_{E2} , as follows,

$$\sigma_{vib}^2 = a \frac{\hbar^2}{2k\mu T_{E1}} \coth\left[\frac{T_{E1}}{2T}\right] + (1-a) \frac{\hbar^2}{2k\mu T_{E2}} \coth\left[\frac{T_{E2}}{2T}\right]. \quad (3)$$

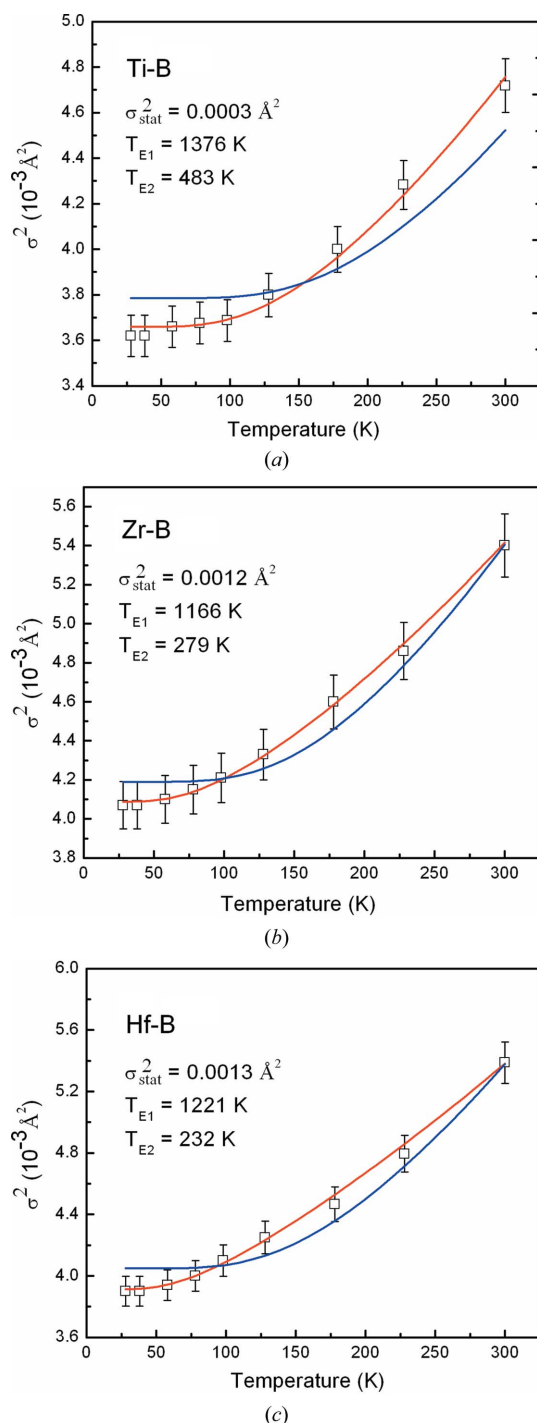
Here a is a parameter describing the degree of uncorrelation of the TM–B pair, and $\mu = m_B m_{TM} / (m_B + m_{TM})$ is the reduced mass of TM and B atoms. Using the above model combined with the classical equation (1) we obtained the DWF temperature-independent behavior of TM–B bonds for all diborides, as shown in Fig. 6. Actually, σ_{stat}^2 , *i.e.* the static disorder, and the two temperatures are summarized in Table 2. At the two temperatures we may associate a corresponding frequency and, as expected, the higher one may be associated with vibration in the layers of B atoms and the lower can be associated with the TM layer atoms. Indeed, the lighter B atoms may vibrate at high frequency, while heavier TM atoms exhibit relatively low vibrational frequencies. We will demonstrate below that the vibrational behavior of B and metal atoms may be separated through a precise determination of the DWF of the TM–B pair from the temperature-dependent EXAFS data.

A complete decoupling of the vibration of the TM–B pairs is possible looking at the parameter a in equation (3). Table 3 compares the values of the parameter a for the three diborides, TiB_2 , ZrB_2 and HfB_2 , together with the μ/a and $\mu/(1-a)$ values. A large difference exists between μ/a and m_B and $\mu/(1-a)$ and m_{TM} for TiB_2 while μ/a and $\mu/(1-a)$ are close to m_B and m_{TM} for both ZrB_2 and HfB_2 . This behavior supports a description of the vibrational behavior of the TM–B pairs of equation (3) through the modified model,

$$\sigma_{vib}^2 = \frac{\hbar^2}{2km_B T_{E1}} \coth\left[\frac{T_{E1}}{2T}\right] + \frac{\hbar^2}{2km_{TM} T_{E2}} \coth\left[\frac{T_{E2}}{2T}\right], \quad (4)$$

that represents the superposition of boron and metal vibrations. Equation (4) suggests the occurrence of a significant decoupling between the vibrations of TM–B bonds in diborides containing heavy transition metals, such as the ZrB_2 and HfB_2 compounds.

A strong correlation typically occurs in the cation–anion bond owing to scattering events involving the photo-excited electron among the photo-absorber and coordinated atoms in temperature-dependent EXAFS spectra. For such systems the


Figure 6

Comparison of experimental DWFs (symbols) of the TM–B pair in (a) TiB_2 , (b) ZrB_2 and (c) HfB_2 with the classical Einstein model (blue lines). A modified model with two frequencies (red lines) may fix the disagreement observed with the classical model.

temperature dependence of the DWF exhibits only one vibration frequency for a given atomic pair. On the contrary, in these transition-metal diborides a large mismatch in the localized vibrational mode of the TM–B pair is observed, mainly due to the layered structure of these systems and the large mass difference between the atomic constituents. As addressed above, an anomalous behavior has also been

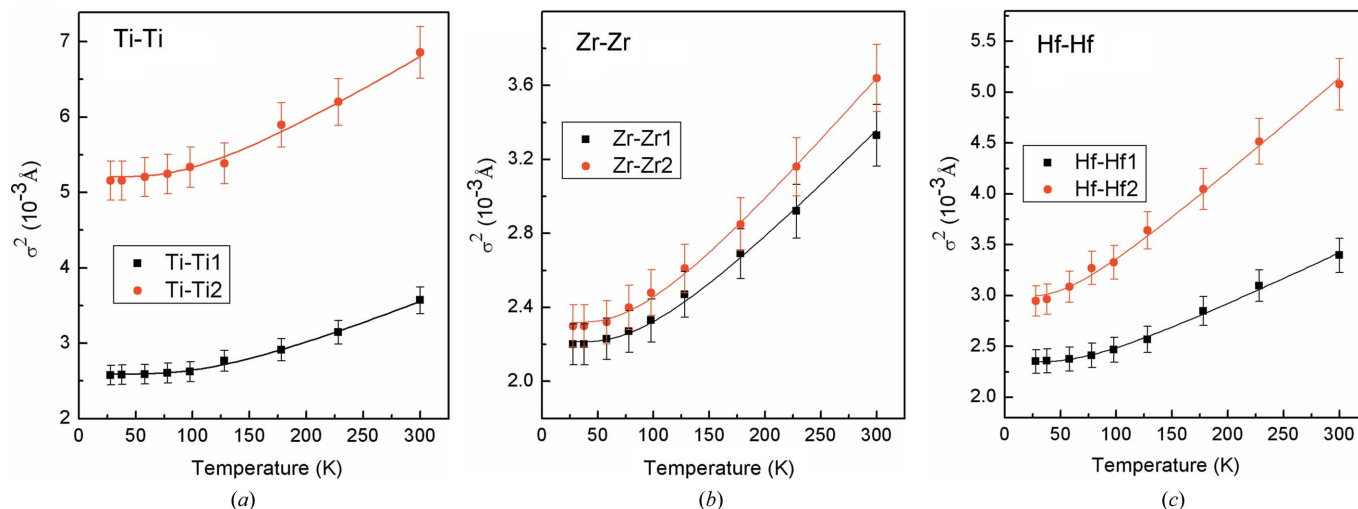
observed in the resistivity and in the specific heat temperature behavior of LaB_6 and other hexaborides and it is compatible with a description where a standard Einstein model referring to the TM matrix combines with a Debye framework describing the lighter boron ions (Mandrus *et al.*, 2001).

These transition-metal diborides are usually considered as reference compounds for the superconductive mechanism of MgB_2 , and the decoupling of the localized vibrational mode of the cation–anion bond that we detected using temperature-dependent EXAFS is an important result. The presence of a strong coupling between metal and boron in diboride systems could be used to correlate the different superconductivity properties exhibited in these diborides. Indeed, our data show that the heavier the metal mass the stronger the vibrational decoupling and, although it cannot be probed by EXAFS, it seems reasonable that a strong vibrational coupling occurs between B and Mg atoms owing to their comparable masses.

MgB_2 and also TMB_2 systems are characterized by nine independent vibrational modes: three acoustic modes with low vibrational frequencies and six optical modes with high vibrational frequencies. The phonon density of states (PDOS) in both MgB_2 and other transition-metal diborides has been measured by inelastic neutron scattering experiments (Osborn *et al.*, 2001; Heid *et al.*, 2003), which, however, do not return information about the correlation of the localized vibration like temperature-dependent EXAFS experiments. The highest and the lowest vibrational frequencies of the PDOS spectra of TiB_2 , ZrB_2 and HfB_2 are reported in the last column in Table 2. These two latter frequencies are in good agreement with the temperature obtained by the inelastic neutron scattering. The correspondence supports the hypothesis that the low-frequency vibrational mode is an acoustic mode related to the collective vibration of transition-metal atoms, while the high-frequency mode is an optical mode corresponding to B-atom vibrations. Moreover, diboride EXAFS data show that, contrary to the behavior of the acoustic mode, the vibrational frequency of the optical mode does not monotonously decrease with the metal mass. Nevertheless, the optical frequencies of these group IV transition-metal diborides monotonously change with the bond length of the B–B bonds, *i.e.* 1.773, 1.846 and 1.828 Å in TiB_2 , ZrB_2 and HfB_2 , respectively. The different behaviors between the optical and acoustic modes as a function of the metal mass also supports the hypothesis of a vibrational decoupling among B and metal atoms.

3.3. Localized vibrations of the TM–TM bonds

Owing to the element sensitivity of EXAFS, local vibrations at different sites can be investigated *versus* temperature. In our EXAFS investigation the second feature of the Fourier transform can be used to extract information about TiB_2 , ZrB_2 and HfB_2 . It contains data regarding the localized vibrations of TM–TM pairs although, because of the layered structure of AlB_2 -type diborides, the TM–TM shell includes two different subshells. These two subshells refer to two different bonding types, *i.e.* the TM1–TM1 (within the layer plane) and the


Figure 7

Comparison of the experimental DW factors (symbols) of the TM–TM pair in (a) TiB_2 , (b) ZrB_2 and (c) HfB_2 with calculations (continuous lines) using the classical Einstein model.

TM2–TM2 (out of the plane), respectively. If we assume that the collective vibration of metal atoms in the system represents the acoustic mode of the lattice vibration, then the three acoustic modes of the diboride lattice vibrations can be detected by EXAFS *versus* temperature taking into consideration that mode in the layer is doubly degenerate.

Because of their layered structure, the collective vibration of the lattice of AlB_2 -type diborides should exhibit a clear anisotropy affected by the metal composition. The compounds we investigated present a similar electronic structure independent of metal masses. In Fig. 7 we show the temperature behavior of the DWFs of the TM–TM1 (solid squares) and TM–TM2 (solid circles) of these diborides successfully reproduced within the framework of the standard Einstein model (equation 2). Moreover, both σ_{stat}^2 , the static disorder contribution, and the Einstein temperatures of the TM–TM1 and TM–TM2 pairs are listed in Table 4. As expected for such compounds, vibrational frequencies within the layers are larger than those out of the plane, supporting a strong interaction of the TM–TM bonds inside the layer with respect to those out of the plane. However, we have to emphasize that the anisotropies do not scale with the metal mass and are larger in the HfB_2 and smaller in the ZrB_2 . Without information on the MgB_2 system, it is impossible from these systems alone to establish a relationship between the anisotropy of the lattice vibration and superconducting behavior of diboride systems.

4. Conclusions

The localized vibrational properties of TiB_2 , ZrB_2 and HfB_2 diboride compounds with group IV TMs have been investigated by temperature-dependent EXAFS experiments. The temperature vibrational behavior investigated on the basis of the standard Einstein model showed an anomalous behavior

Table 4

Calculated static distortions and corresponding Einstein temperatures of the TM–TM1 and TM–TM2 shells for the investigated diborides.

	Bonding	R (Å)	σ_{stat}^2 (Å ²)	T_E (K)	ν' (meV)	$T_E(\text{TM-TM1})/T_E(\text{TM-TM2})$
TiB_2	Ti–Ti1	3.07	0.0013	385 ± 25	33.2 ± 2.2	0.84
	Ti–Ti2	3.26	0.0036	325 ± 25	28.0 ± 2.2	
ZrB_2	Zr–Zr1	3.19	0.0013	288 ± 15	24.8 ± 1.3	0.94
	Zr–Zr2	3.55	0.0013	272 ± 15	23.4 ± 1.3	
HfB_2	Hf–Hf1	3.17	0.0017	224 ± 15	19.3 ± 1.3	0.75
	Hf–Hf2	3.50	0.0022	168 ± 15	14.4 ± 1.3	

and a strong anisotropy. While an analysis of the EXAFS signals from the TM–TM bonds can be extracted and described by a standard Einstein model, the DWF of the TM–B pairs is characterized by an anomalous temperature behavior that strongly supports the occurrence of an additional low-frequency phonon mode and may be described by a modified equation with two temperatures.

The anomalous behavior detected in these transition-metal diborides serves as an important reference for the investigation of the superconductive mechanism of MgB_2 , and supports the existence of decoupled localized vibrational modes associated with cation–anion bonds with large cation–anion mass differences. Our EXAFS results are consistent with other experimental data and may explain why superconductivity is not observed in these transition-metal compounds.

This work was partly supported by the National Outstanding Youth Fund (Project No. 10125523 to ZW), the Key Important Nano-Research Project (90206032) of the National Natural Science Foundation of China and the Knowledge Innovation Program of the Chinese Academy of Sciences (KJ CX2-SW-N11).

References

An, J. M. & Pickett, W. E. (2001). *Phys. Rev. Lett.* **86**, 4366–4369.

- Buzea, C. & Yamashita, T. (2001). *Supercond. Sci. Technol.* **14**, R115–R146.
- Dalba, G. & Fornasini, P. (1997). *J. Synchrotron Rad.* **4**, 243–255.
- Gasparov, V. A., Sidorov, N. S., Zver'kova, I. I. & Kulakov, M. P. (2001). *JETP Lett.* **73**, 601–604.
- Gregor, R. B. & Lytle, F. W. (1979). *Phys. Rev. B*, **20**, 4902–4907.
- Heid, R., Renker, B., Schober, H., Adelman, P., Ernst, D. & Bohnen, K. P. (2003). *Phys. Rev. B*, **67**, 180510.
- Hinks, D. G., Claus, H. & Jorgensen, J. D. (2001). *Nature (London)*, **411**, 457–460.
- Ivanovskii, A. L. (2003). *Phys. Solid State*, **45**, 1829–1859.
- Knap, G. S., Pan, H. K. & Tranquada, J. M. (1985). *Phys. Rev. B*, **32**, 2006–2009.
- Kortus, J., Mazin, I. I., Belashchenko, K. D., Antropov, V. P. & Boyer, L. L. (2001). *Phys. Rev. Lett.* **86**, 4656–4659.
- Lannin, J. S. & Messier, R. (1980). *Phys. Rev. Lett.* **45**, 1119–1122.
- Lytle, F. W., Sayers, D. E. & Stern, E. A. (1989). *Proceedings of the 5th International Conference on X-ray Absorption Fine Structure (XAFS V)*, Seattle, USA, 22–26 August 1988.
- Mandrus, D., Sales, B. C. & Jin, R. (2001). *Phys. Rev. B*, **64**, 012302.
- Nagamatsu, J., Nakagawa, N., Muranaka, T., Zenitani, Y. & Akimitsu, J. (2001). *Nature (London)*, **410**, 63–64.
- Naidyuk, Yu. G., Kvitnitskaya, O. E., Yanson, I. K., Drechsler, S.-L., Behr, G. & Otani, S. (2002). *Phys. Rev. B*, **66**, 140301.
- Newville, M., Livins, P., Yacoby, Y., Rehr, J. J. & Stern, E. A. (1993). *Phys. Rev. B*, **47**, 14126–14131.
- Osborn, R., Goremychkin, E. A., Kolesnikov, A. I. & Hinks, D. G. (2001). *Phys. Rev. Lett.* **87**, 017005.
- Rehr, J. J., Mustre, J., Zabinsky, S. I. & Albers, R. C. (1991). *J. Am. Chem. Soc.* **113**, 5135–5140.
- Ressler, T. (1998). *J. Synchrotron Rad.* **5**, 118–122.
- Sevillano, E., Meuth, H. & Rehr, J. J. (1979). *Phys. Rev. B*, **20**, 4908–4911.
- Stern, E. A., Newville, M., Ravel, B., Yacoby, Y. & Haskel, D. (1995). *Physica B*, **208/209**, 117–120.
- Vajeeston, P., Ravindran, P., Ravi, C. & Asokamani, R. (2001). *Phys. Rev. B*, **63**, 045115.
- Yildirim, T. *et al.* (2001). *Phys. Rev. Lett.* **87**, 037001.
- Zabinsky, S. I., Rehr, J. J., Ankudinov, A., Albers, R. C. & Eller, M. J. (1995). *Phys. Rev. B*, **52**, 2995–3009.